Chemical Science

ROYAL SOCIETY OF CHEMISTRY

EDGE ARTICLE

View Article Online
View Journal | View Issue

Cite this: *Chem. Sci.*, 2023, **14**, 514

All publication charges for this article have been paid for by the Royal Society of Chemistry

Heavy metalla vinyl-cations show metal–Lewis acid cooperativity in reaction with small molecules (NH_3, N_2H_4, H_2O, H_2)†

Maximilian Auer,[a] Janina Bolten,[a] Klaus Eichele,[a] Hartmut Schubert,[a] Christian P. Sindlinger *[b] and Lars Wesemann *[a]

Halide abstraction from tetrylidene complexes [TbbE(Br)IrH(PMe_3)$_3$] [E = Ge (**1**), Sn (**2**)] and [Ar*E(Cl)IrH(PMe_3)$_3$] gives the salts [TbbEIrH(PMe_3)$_3$][BAr^F_4] [E = Ge (**3**), Sn (**4**)] and [Ar*EIrH(PMe_3)$_3$][BAr^F_4] [E = Ge (**3′**), E = Sn (**4′**)] (Tbb = 2,6-[CH($SiMe_3$)$_2$]$_2$-4-(*t*-Bu)C_6H_2, Ar* = 2,6-$Trip_2C_6H_3$, Trip = 2,4,6-triisopropylphenyl). Bonding analysis suggests their most suitable description as metalla-tetrela vinyl cations with an Ir=E double bond and a near linear coordination at the Ge/Sn atoms. Cationic complexes **3** and **4** oxidatively add NH_3, N_2H_4, H_2O, HCl, and H_2 selectively to give: [TbbGe(NH_2)IrH_2(PMe_3)$_3$][BAr^F_4] (**5**), [TbbE($NHNH_2$)IrH_2(PMe_3)$_3$][BAr^F_4] [E = Ge (**7**), Sn (**8**)], [TbbE(OH)IrH_2(PMe_3)$_3$][BAr^F_4] [E = Ge (**9**), Sn (**10**)], [TbbE(Cl)IrH_2(PMe_3)$_3$][BAr^F_4] [E = Ge (**11a**), Sn (**12a**)], [TbbGe(H)IrH_2(PMe_3)$_3$][BAr^F_4] (**13**), [TbbSn(μ-H_3)Ir(PMe_3)$_3$][BAr^F_4] (**14**), and [TbbSn(H)IrH_2(PMe_3)$_3$][BAr^F_4] (**15**). **14** isomerizes to give **15** *via* an 1,2-H shift reaction. Hydride addition to cation **3** gives a mixture of products [TbbGeHIrH(PMe_3)$_3$] (**16**) and [TbbGeIrH_2(PMe_3)$_3$] (**17**) and a reversible 1,2-H shift between **16** and **17** was studied. In the tin case **4** the dihydride [TbbSnIrH_2(PMe_3)$_3$] (**18**) was isolated exclusively. The PMe_3 and PEt_3 derivatives, **18** and [TbbSnIrH_2(PEt_3)$_3$] (**19**), respectively, could also be synthesized in reaction of [TbbSnH_2]$^-$ with the respective chloride [(R_3P)$_n$IrCl] (R = Me, *n* = 4; R = Et, *n* = 3). Reaction of complex **19** with CO gives the substitution product [TbbSnIrH_2(CO)(PEt_3)$_2$] (**20**). Further reaction with CO results in hydrogen transfer from the iridium to the tin atom to give [TbbSnH_2Ir(CO)$_2$(PEt_3)$_2$] (**21**). The reversibility of this ligand induced reductive elimination transferring **20** to **21** is shown.

Received 10th October 2022
Accepted 24th November 2022

DOI: 10.1039/d2sc05620h

rsc.li/chemical-science

Introduction

Tetrylidyne complexes are heavier homologs of the parent carbyne complexes and exhibit a triple bond between a low-valent Group 14 element and a transition metal.[1] With the synthesis of [Cp(CO)$_2$Mo≡GeAr′] Power and co-workers have reported a pioneering example featuring a Mo≡Ge triple bond with a nearly linear C–Ge≡Mo unit.[2,3] Filippou *et al.* developed the chemistry of the tetrylidyne coordination compounds and presented a broad variety of fascinating examples exhibiting a central triple bond unit M≡E with combinations between elements: M = Nb, Cr, Mo, W, Mn, Re, Fe, Ni, Pt and E = Si, Ge, Sn, Pb.[4–19] The following synthetic procedures for tetrylidyne complexes were presented in the literature (Scheme 1): (1) starting with a metalloylidene complex, elimination of transition metal coordinated carbon monoxide yields the tetrylidyne complex;[2,3,6,20] (2) addition of organotetrylene halides to transition metal complexes and elimination of

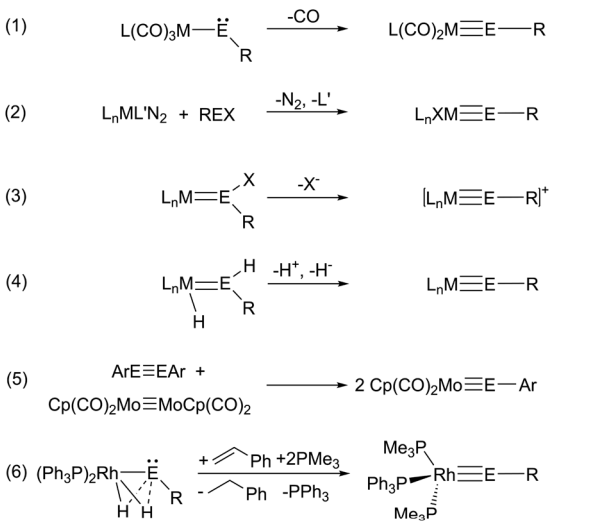

Scheme 1 Syntheses of tetrylidyne metal complexes (X = halide, hydride; L′ = N_2, phosphine).

[a]*Institut für Anorganische Chemie, Auf der Morgenstelle 18, 72076 Tübingen, Germany. E-mail: lars.wesemann@uni-tuebingen.de*

[b]*Institut für Anorganische Chemie, Universität Stuttgart, Pfaffenwaldring 55, 70569 Stuttgart, Germany. E-mail: christian.sindlinger@iac.uni-stuttgart.de*

† Electronic supplementary information (ESI) available. CCDC 2208289–2208301. For ESI and crystallographic data in CIF or other electronic format see DOI: https://doi.org/10.1039/d2sc05620h

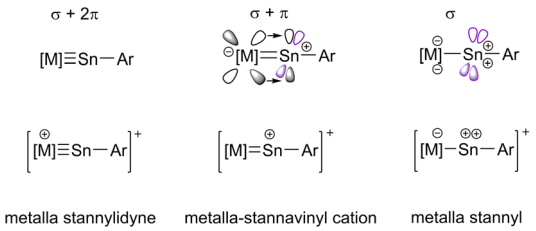

Scheme 2 Bonding in stannylidyne complexes, continuum of π-backbonding. (Violet coloured orbital at Sn: without backdonation from transition metal).

nitrogen or phosphine ligands;[5,8,9,12–19] (3) halide, hydride or NHC abstraction from ylidene complexes;[4,7,10,11,21–24] (4) Tobita *et al.* reported dehydrogenation or stepwise proton and hydride abstraction;[25–28] (5) metathetical exchange between metal–metal triple bonds;[29] (6) hydrogen transfer in reaction of dihydride complexes with styrene.[30]

The metal-element triple bond usually consists of a σ-bond derived from the donation of a Group 14 element lone pair to the transition metal and two π-bonds, which result from transition metal d-orbital donation into the empty p-orbitals at the Group 14 element.[19,24] In this continuum (Scheme 2) of π-backbonding interactions the electronic situation of the participating fragments play a key role and can give rise to potential fluctional internal frustration resulting in increased reactivity of the multiple bond.[23]

Results and discussion

Motivated by our recent progress in tetrylidyne rhodium chemistry we started a project to investigate multiple bonds between iridium and heavy Group 14 elements.[30] In our initial efforts we reacted low valent organo element bromides of germanium $[(TbbGeBr)_2]$ and tin $[TbbSnBr_2][Li(thf)_2]$ with the iridium hydride $[(Me_3P)_4IrH]$ (Scheme 3 and Table 1).[31,32,33] A phosphine was substituted against the bromoorgano tetrylene and the tetrylidene compounds $[(TbbBrE)IrH(PMe_3)_3]$ (E = Ge: **1**, E = Sn: **2**, see Scheme 3 for depiction) were obtained in high yield (**1**: 96%, **2**: 95%). In the case of the germanium derivative **1**, determination of the molecular structure in the solid state was possible (see Table 2 and ESI† for details). The Ir–Ge distance in **1** of 2.2879(3) Å is a short distance between these elements (for comparison $[\{PhB(CH_2PPh_2)_3\}IrH_2GeMes_2]$ [Ge–Ir 2.339(1) Å],[34–36] based on a CSD search, a shorter Ir–Ge interatomic distance was not reported) and the Ge atom shows a trigonal planar arrangement. Therefore, the bonding situation in the Ge–Ir complex was also investigated using DFT calculations in combination with NBO[37] analysis, pointing toward a germylene acting as a σ-donor and π-acceptor ligand (see ESI†).[38,39] The stannylene complex **2** exhibits a characteristic signal in the ^{119}Sn-NMR spectrum at 566 ppm indicative for stannylene coordination.[40,41] To synthesize the desired tetrylidyne iridium complexes, elimination of HBr was explored for both complexes **1** and **2**. However, these experiments with strong bases like benzyl-potassium, KO^{t}Bu or Ph_3CLi, were not successful. Instead, halide abstraction with $Na[BAr^F{}_4]$ was straightforward (Scheme 3) and the cationic iridium hydride complexes were isolated as $[BAr^F{}_4]$-salts in high yield (**3** Ge: 89%, **4** Sn: 88%). Examples of cationic transition metal hydride complexes featuring an M–E multiple bond with Group 14 elements are present in the literature (IrH–Si,[42,43] MoH–Si,[21] FeH–Sn,[23] and OsH–Si[22]).

In the crystalline state both products **3** and **4** exhibit a major disorder of the entire molecule and poor crystallinity. The TbbSn derivative **4** and the Ar*Ge complex **3′** (the terphenyl substituent Ar* was also employed to check for possible non-disordered structures of **3′** and **4′**; Ar* = 2,6-$Trip_2C_6H_3$, Trip = 2,4,6-triisopropylphenyl) are shown in Fig. 2. Syntheses of **3′** and **4′** were carried out using analogous starting materials and comparable procedures (see ESI† for details). However, in the

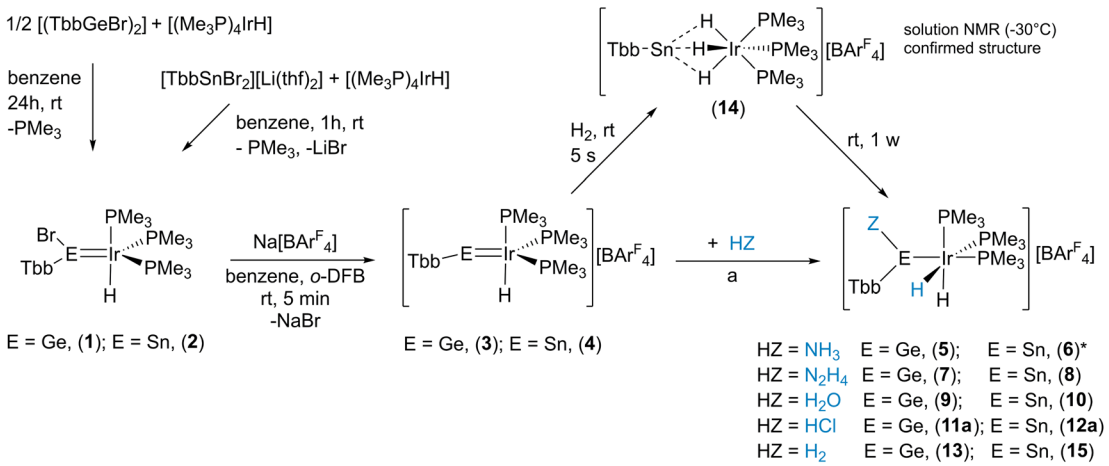

Scheme 3 Syntheses of **1**, **2** and bromide abstraction to give tetrylidinium coordination compounds **3**, **4**. Reactivity studies of tetrylidinium–iridium cations (**3**, and **4**). a: HZ = NH_3 : NH_3 (g), benzene/*o*-DFB 0.3/0.05 mL, rt, 5 s; HZ = N_2H_4 : N_2H_4 (1 M thf), benzene/*o*-DFB 1 : 1, rt, 5 s; HZ = H_2O : $BaCl_2{\cdot}H_2O$, *o*-DFB, rt, 1 h; HZ = HCl : $HCl{\cdot}Et_2O$ (1 M), *o*-DFB, rt, 5 s; HZ = H_2 : H_2, rt 24 h (E = Ge). **(6)***: **6** was not isolated, instead a reaction mixture between **4** and excess NH_3 was characterized (*vide infra*). [*o*-DFB = 1,2-difluorobenzene, $Ar^F = C_6H_3$-3,5-$(CF_3)_2$].

Table 1 Selected NMR data

	^{1}H Ir–H δ	$^2J_{SnH}$	$^2J_{PH}$	$^2J_{HH}$	^{1}H E–Hδ	J_{SnH}	$^2J_{PH}$	J_{HH}	^{31}P δ	$^2J_{SnP}$	^{119}Sn δ	$^2J_{SnP}$	J_{SnH}	δ calc.
1	−11.82	20.8							−45.6					
2	−12.65	219	18.6						−43.7	598	566	603	218	
3	−11.87	8.8							−43.9					
4	−11.30	119	10.3						−38.5	347	1424, 1284 Solid	347	Broad	1449
5	−12.80								−62.3, −53.8					
4/NH_3	−13.67	127	11.4						−60.9, −50.1	135, 1827	−11	1831	Broad	[a]
7	−13.03								−62.3, −53.7					
8	−13.47	251							−60.1, −45.5	144, 1680	604	1682, 142		673.8
9	−12.69								−58.7, −51.9					
10	−13.29								−56.3, −43.8	124, 1714	648	1730, 128		778.4
11a	−11.21								−57.5, −50.9					
12a	−12.98	255							−57.5, −42.6	119, 144 1714, 1777	772	1784, 126		
13	−11.90				13.98		32.6, 7.6		−54.0, −48.8					
14	−7.94	265							−45.2		1592	Broad		
15	−12.67	195			18.59	772	37.5, 4.7		−54.9, −41.6	104, 1509	1013	1496	775	
16	−10.79				12.04		13.6	3.5	−42.1 Broad					
17	−11.07								−58.8, −30.0					
18	−12.10								−60.9, 24.4	209, 320	3835	327		
19	−13.26								−26.4, 62.1		3827	458		
20	−10.49		21.3, 15.6	3.7					−17.1, 42.9	336	3321	336		
	−9.83		109, 17.1	3.7										
21									−16.5	320, 305	−388	320	1406	

[a] ^{119}Sn DFT calculations of $[TbbSn(NH_2)IrH_2(PMe_3)_3]^+$, calc. 709 ppm; $[TbbSn(NH_3)(NH_2)IrH_2(PMe_3)_3]^+$, calc. 88 ppm.

case of **4′** we also developed a further synthesis employing the cation $[Ar^*Sn]^+$ reacting as a nucleophile substituting a phosphine ligand (Scheme 4). In the molecular structures of **3′** and **4** the absence of the bromide and the large C–E–Ir angle (>160°) are characteristic features for these cations. The found interatomic distances of Ge–Ir 2.225(2) Å and Sn–Ir 2.4135(5) Å are short bond lengths between these elements (Table 2).[34,44–47] (The data of **3′** and **4** are results of disordered structures, **4**: distance of the 90% component is shown).

In the ^{1}H NMR spectrum the signal for the hydride was observed at low frequencies (Tables 1 and 3: *q*, −11.87 ppm, $^2J_{P–H}$ = 8.8 Hz; **4**: *q*, −11.30 ppm + sat., Ir*H*, $^2J_{P–H}$ = 10.3 Hz, $^2J_{Sn–H}$ = 119 Hz) and in the ^{119}Sn NMR spectrum of **4** (solution as well as solid state NMR data) a shift to high frequencies (1424 ppm) in comparison to starting material **2** was observed (Table 1). In compounds **1–4**, the Ir atom is trigonally bipyramidally coordinated by three phosphine ligands, a hydride, and the Group 14 moiety. However, the hydride signal in the ^{1}H NMR spectrum featuring a quartet due to coupling with the ^{31}P nuclei and the ^{31}P-NMR spectrum showing one resonance for the three phosphine ligands indicate time averaged high symmetry of compounds **1–4**. To evaluate the presumed dynamic process in solution, temperature dependent NMR spectroscopy was carried out. Because the solubility of salts **3** and **4** was limited at low temperatures and compounds **1–4** exhibit the same ligand arrangement at iridium and comparable Ir–H hydride resonances and ^{31}P NMR spectra low temperature experiments were carried out with a sample of **1**.

Variable temperature ^{31}P{^{1}H} and ^{1}H NMR studies of **1** at 11.75 T indeed demonstrate fluxional behavior (Fig. 1). At 299.7 K, this process makes the three phosphine ligands chemically and magnetically equivalent, resulting in a singlet in the ^{31}P{^{1}H} and a quartet in the ^{1}H NMR spectra. However, cooling the sample to 190.0 K slows down the exchange sufficiently such that no phosphine ligand exchange is measurable and the ^{31}P{^{1}H} NMR spectrum corresponds to an AB_2, the ^{1}H NMR spectrum to an AB_2X spin system. One rare conspicuous feature of the AB_2X spin system is the asymmetry within the multiplet, partially reproduced by the simulation (Fig. 1b, bottom). It depends on the ratio of the coupling constants to the shift difference δ_{AB}, as well as on the relative signs of these parameters.[48–50] Given that the sign of δ_{AB} is known from ^{31}P NMR spectroscopy, the signs of the coupling constants are absolute. Additional spectra and simulations at intermediate temperatures are collected in the ESI.†

The short Ir–E bond length and particularly the crystallographically confirmed large Ir–E–C angle of *ca.* 160° are indicative for a tetrylidyne moiety and we were interested in addressing the bonding situation computationally by means of DFT. Interestingly, standard structure optimizations with a usually robust functional for organometallics such as BP86 (including dispersion corrections) fail completely to reproduce this large angle and predict (for example for tin compound **4**) an Ir–Sn–C angle of 120°, along with a deviating T-shape geometry of the phosphine ligands at the Ir-atom. Such small angles would instead be more indicative of metallo-stannylene rather than a metallastannylidyne. Hybrid or range separated

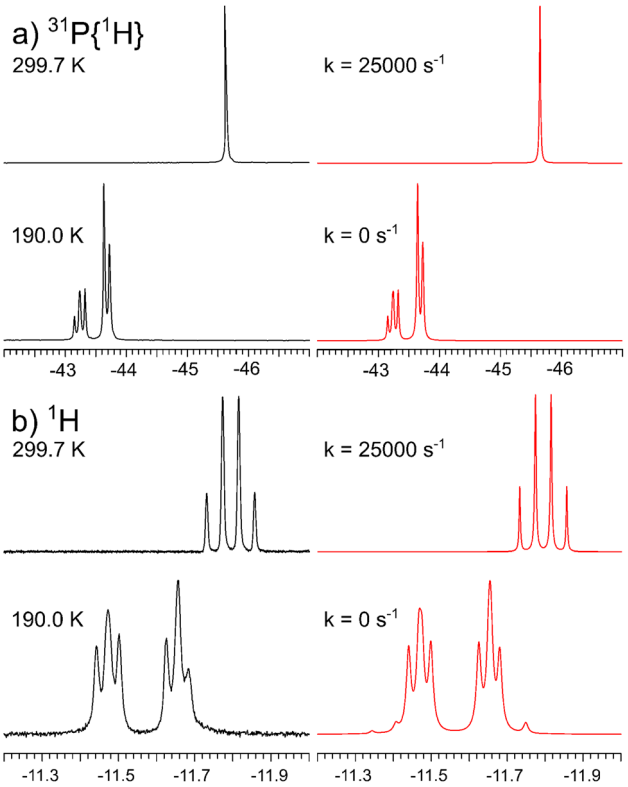

Fig. 1 Experimental (left) and simulated (right) variable temperature (a) 202.46 MHz $^{31}P\{^{1}H\}$ and (b) 500.13 MHz ^{1}H NMR spectra of **1**.

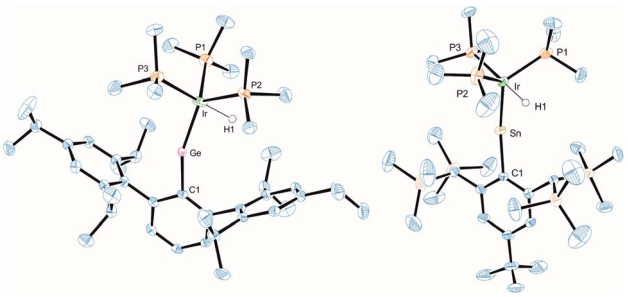

Fig. 2 ORTEP of the molecular structure of the cation of **3′** and **4**. Ellipsoids set at 50% probability. Hydrogen atoms except Ir–H are omitted for clarity. For selected interatomic distances and angles see Table 2.

functionals such as M06-2X or ωB97X however optimized to local minima with angles around 160°. Compared to this experimental structure with a more linear coordination environment as also found by ωB97X, the more bent metallo-stannylene isomer structure (predicted by BP86 optimizations)

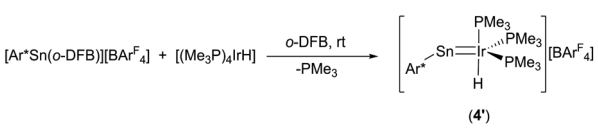

Scheme 4 Synthesis of **4′** *via* substitution.

was found the more stable structure by both model chemistries by respective single-point calculations. However, the extent of favourisation of the more bent-structure differed significantly between the two functionals (17.2 kcal mol^{-1} BP86; 2.7 kcal mol^{-1} ωB97X).

To finally corroborate the validity of the linear structure model as the dominant species beyond the single experimental data point from the X-ray geometry, we compared computationally predicted ^{119}Sn-NMR chemical shifts and their anisotropic shielding tensors (Table 3) with the experimentally determined isotropic shifts from solution as well as from solid-state NMR-spectroscopy. The experimental isotropic shift of $\delta_{exp}(^{119}Sn)$ = 1424 ppm (solution)/1284 ppm (solid state) is computationally (ADF2022, revPBE/TZ2P) very well reproduced for optimized structures in which the experimental angle (*ca.* 160°) was constrained ($\delta_{comp}(^{119}Sn)$ = 1449 ppm) as opposed to freely optimised structures with a metallo-stannylene-type angle (*ca.* 120°, $\delta_{comp}(^{119}Sn)$ = 2125 ppm). Moreover, the respective computational anisotropic magnetic shielding tensor (Table 3) matches the experimentally approximated tensor from ^{119}Sn-solid-state NMR. This further experimental insight corroborates the anticipated relevance of the near-linear structure both in solid state and in solution.

Due to the ambiguity in the computational reproduction of the nature of the Ir–E interaction, we further probed the electronics by means of EDA-NOCV analysis and NBO analysis of a reduced model system $[(Me_3P)_3(H)Ir–Sn–Me]^+$. Again, BP86 optimizes to a strongly bent structure (Ir–Sn–Me angle 107°) where ωB97X predicts an almost linear structure (172°). This probe with essentially non-bulky Me-substituents indicates that influences of dispersion or ligand repulsion are not key to the structural differences observed and that electronics must play a decisive role. NBO analysis (ωB97X-def2-SVP/TZVP(Sn,Ir)) of $[(Me_3P)_3(H)Ir–Sn–Me]^+$ with an Ir–Sn–C angle constrained to the experimental value (160°) suggests a separation into trigonal-bipyramidal d^8-$[Ir(H)(PMe_3)_3]$ and $[:Sn–Me]^+$ fragments with only very weak and very polarised bonding interactions of a σ-donating s-orbital based Sn-lone pair of electrons into a sd-hybrid orbital at the iridium atom, and only one inversely polarised π-backdonation from an Ir-d-orbital into one empty p-orbital at the Sn-atom, leaving an empty p-orbital at the tin atom (Fig. 3).

EDA-NOCV analyses (ωB97X-def2-SVP/TZVP(Sn,Ir)) on the same structure with a respective fragment partitioning of a neutral $[Ir(H)(PMe_3)_3]$ fragment and a cationic $[:Sn–Me]^+$ gave an essentially identical picture with three leading interactions (see the ESI† for further details). The deformation densities of these interactions are shown in Fig. 4. Energetically, the π-backdonation contributes almost equally to the overall Sn–Ir bonding as the σ-donation contribution which is, for symmetry reasons, divided into two individual NOCV-contributions.

From this computational insight, we conclude that there is no true triple-bonding between Ir and Sn but rather a double bond comprising of one σ- and one π-bond and an empty p-orbital at a near-linear coordinate Sn-atom with the cationic charge primarily residing at the Sn-atom. We would thus propose to see this moiety as a (metalla-)stannavinyl cation.

Table 2 Selected data of molecular structures **1**, **3′**, **4**, **5**, **7**, **9**, **10**, **12b**, **13**, **19–21**[a]

	Ir–E	E–X	E–C	Ir–E–C	Ir–P1	Ir–P2	Ir–P3	Ir–C2	C2–O1
1 E = Ge, X = Br	2.2879(3)	2.4562(4)	1.982(3)	140.8(1)	2.2687(10)	2.2791(9)	2.3157(9)		
3′ E = Ge	2.225(2)		1.948(4)	158.8(4)	2.2906(12)	2.2868(12)	2.3166(14)		
4 E = Sn	2.4135(5)		2.133(5)	159.2(1)	2.2759(15)	2.2832(15)	2.3400(13)		
5 E = Ge, X = NH_2	2.3538(4)	1.778(2)	1.944(2)	130.9(1)	2.3365(7)	2.3092(7)	2.3345(7)		
7 E = Ge, X = N_2H_3	2.3492(4)	1.792(4)	1.957(4)	129.8(1)	2.3543(12)	2.3075(11)	2.3372(10)		
9 E = Ge, X = OH	2.3344(3)	1.770(2)	1.948(3)	134.9(1)	2.3421(8)	2.3524(8)	2.3052(8)		
10 E = Sn, X = OH	2.5078(4)	1.995(3)	2.126(2)	138.89(7)	2.3389(10)	2.2849(9)	2.3508(9)		
12b E = Sn, X = Br	2.5167(3)	2.5387(6)	2.130(4)	137.36(11)	2.3463(11)	2.2955(12)	2.3351(12)		
13 E = Ge, X = H	2.3400(6)	1.66(6)	1.946(5)	130.8(1)	2.3394(15)	2.3428(15)	2.3151(15)		
19 E = Sn	2.6353(2)		2.229(3)	115.0(1)	2.3414(7)	2.3249(6)	2.3400(7)		
20 E = Sn	2.5968(3)		2.207(3)	106.6(1)	2.3209(9)	2.4164(10)		1.891(6)	1.144(8)
21 E = Sn, X = 2H	2.6598(2)	1.78(2)	2.181(2)	123.5(1)	2.3434(6)	2.3203(7)		1.892(2)	1.156(3)

[a] Molecular structures of **3′**, **4**, **5**, **9**, **10**, **12b**, **13**, **19–21** show a disorder in the solid state.

Table 3 Observed (solid state) and calculated anisotropic ^{119}Sn NMR chemical shift tensor of **4**

[C–Sn–Ir]°	δ_{iso} [ppm]	δ_{11} [ppm]	δ_{22} [ppm]	δ_{33} [ppm]
Exp. (**4**) 160	1284	2622	2622	−978
Calc. 160	1449	3108	2548	−1308
Calc. 120	2125	2467	2127	1780

This cationic nature of the Sn-site may also explain the electrophilicity and regioselective bond-additions in subsequent reactions (*vide infra*).

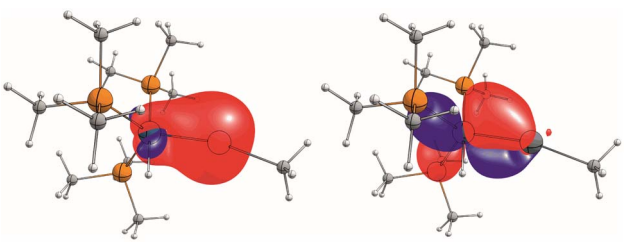

Fig. 3 Depiction of NLMOs with significant contributions of Sn and Ir. Left: 82% Sn (s)/11% Ir (sd); right 83% Ir (d)/13% Sn(p); isovalues at. 0.05 a.u.

To further corroborate our assignment of the charges in the Ir=Ge/Sn cation fragments of **3** and **4**, NPA charges have been computed. In each case (**3** Ge: +0.91/Ir: −0.5; **4** Sn: +1.18/Ir: −0.6) a polar distribution of charges is observed with a clearly negative Ir-atom and positive charge at the tetrel atom. This is in line with our rationale of the experimental observation involving a Lewis-acidic, positively charged tetrel atom as key center of reactiviy in these compounds. A slightly less pronounced distribution in the Ge-case may result from more effective π-overlap and thus increased Ir→Ge electron backdonation.

Because of the interesting bonding situation and electrophilicity of cations [Ge–Ir] **3** and [Sn–Ir] **4** we set up a systematic investigation of their chemical properties. Both cations have a good preparative accessibility [yield of 89% (**3**) and 88% (**4**)] enabling a study of their chemistry. The reactivity of **3** and **4** was explored in reactions with ammonia, hydrazine, water, hydrogen chloride, and hydrogen (Scheme 3). At ambient temperature with ammonia, hydrazine, water, or hydrogen chloride, both cations show a spontaneous heterolytic addition reaction across the E = Ir bond (Scheme 3). Upon heterolysis of the N–H bond, NH_3 and N_2H_4 react with the electrophilic Group 14 element moiety to give an aryl amido/hydrazido tetrylene. The proton adds to the iridium fragment [IrH(PMe_3)$_3$] to result

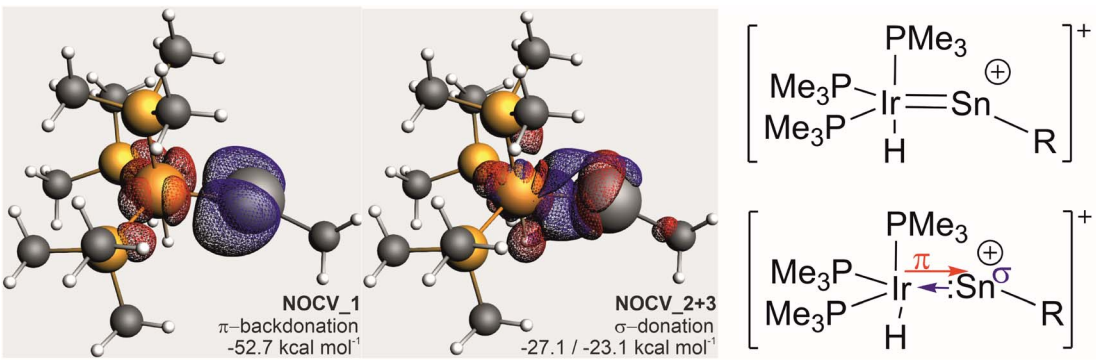

Fig. 4 (Left): Depiction of deformation densities of leading interactions from EDA-NOCV analysis (isovalues at 0.004 a.u.; electron flow: red to blue). NOCV2 and 3 are combined in one depiction. (Right) Proposed leading bonding description for cation **4**.

in a formal oxidation of Ir(I) to Ir(III). The reaction products ([Ge–NH_2] **5**, [Ge–N_2H_3] **7**, [Sn–N_2H_3] **8**) were characterized by NMR spectroscopy and the solid state molecular structures of **5** and **7** were determined by X-ray diffraction (Fig. 5). The Ir–Ge bond lengths found in **5** and **7** (Table 2) can be compared with interatomic Ge–Ir distances found for germylene–iridium coordination compounds.[44,51] The Ge–N bond lengths of addition products [Ge–NH_2] **5** and [Ge–N_2H_3] **7** exhibit Ge–N distances lying in the range [1.76(1) – 1.878(3) Å] of literature examples.[52–58] The Ge atom in **5** and **7** is trigonal planar coordinated, and the iridium atom shows an octahedral ligand arrangement with the phosphine ligand in a facial coordination. DFT calculations using ORCA were performed to evaluate the coordination of the aryl amido- and hydrazido germylene at iridium. Based on the results of NBO analysis a partial delocalization of an electron pair of the NHR-substituent and Ir-fragment into the empty p-orbital at Ge was found (see ESI† for further details). The tin reaction product [Sn–N_2H_3] **8** was also characterized by ^{119}Sn NMR spectroscopy (Table 1) and the chemical shift can be compared with the calculated isotropic shift (**8**: exp. 604 ppm, calc. 674 ppm). In the case of the reaction of **4** with NH_3 a product structure analogous to the germanium NH_3-addition product [Ge-NH_2] **5** was assumed. However, the comparison between experimental ^{119}Sn NMR data of the reaction mixture **4**/excessive NH_3 (exp. −11 ppm) and calculated NMR data based on the optimized structural model of **5** after replacement of the Ge atom against a Sn Atom ([TbbSn(NH_2)$IrH_2(PMe_3)_3$]$^+$, calc. 709 ppm) exhibits a large difference. The low frequency signal of the mixture **4**/NH_3 at −11 ppm points toward an NH_3 adduct [TbbSn(NH_3)(NH_2)$IrH_2(PMe_3)_3$]$^+$ to be present in NMR solutions with excess NH_3. Therefore, this presumed NH_3 adduct [TbbSn(NH_3)(NH_2)$IrH_2(PMe_3)_3$]$^+$ (structure optimized by DFT, ^{119}Sn NMR by ADF: 88 ppm) was calculated by DFT methods and shows a calculated ^{119}Sn NMR chemical shift (88 ppm) in good accordance to the experimental signal (−11 ppm). Furthermore, based on DFT calculations the NH_3 adduct formation is an exergonic ($\Delta G = -3.94$ kcal mol^{-1}, BP86-D3BJ/def2SVP) reaction making the assumption of an adduct formation feasible. However, isolation of this adduct under an atmosphere of ammonia was not possible. The product of hydrolysis, compound **10** [Sn–OH], crystallized at −40 °C after several days.

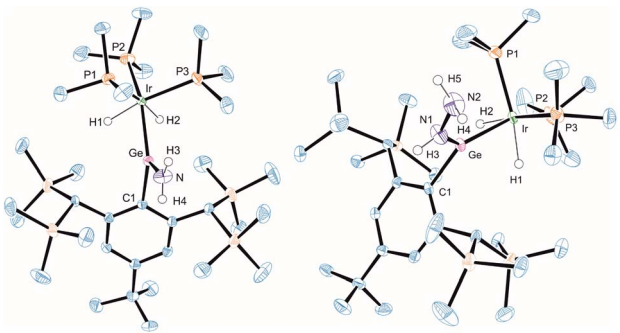

Fig. 5 ORTEP of the molecular structures of **5** and **7**. Ellipsoids set at 50% probability. Hydrogen atoms except N–H and Ir–H are omitted for clarity. For selected interatomic distances and angles see Table 2.

Activation of ammonia and hydrazine is a very active field of research.[59–64] Besides coordination induced bond weakening (Scheme 5e),[59–61] oxidative addition at transition metal complexes[65–69] or main group element compounds[56,57,70–80] (Scheme 5a and b), cooperative reactions with metal–ligand systems[81–85] and a *N*-heterocyclic germylene[55] were reported (Scheme 5c and d). These literature examples of cooperative metal–ligand reactivity exhibit formation of a M–NH_2 moiety (M = Ru, Rh, Ir, Ni; Ge) and transfer of a hydrogen atom to the ligand. Complexes **5**, **7**, **8** are the products of a cooperative heterolytic metal–ligand cleavage of a N–H bond and formation of an Ir–H and E-NHR moiety (R = H, NH_2; E = Ge, Sn) was observed (Scheme 3).[86,87] Obviously, the cations [Ge–Ir] **3** and [Sn–Ir] **4** exhibit metal–ligand cooperativity with the main group

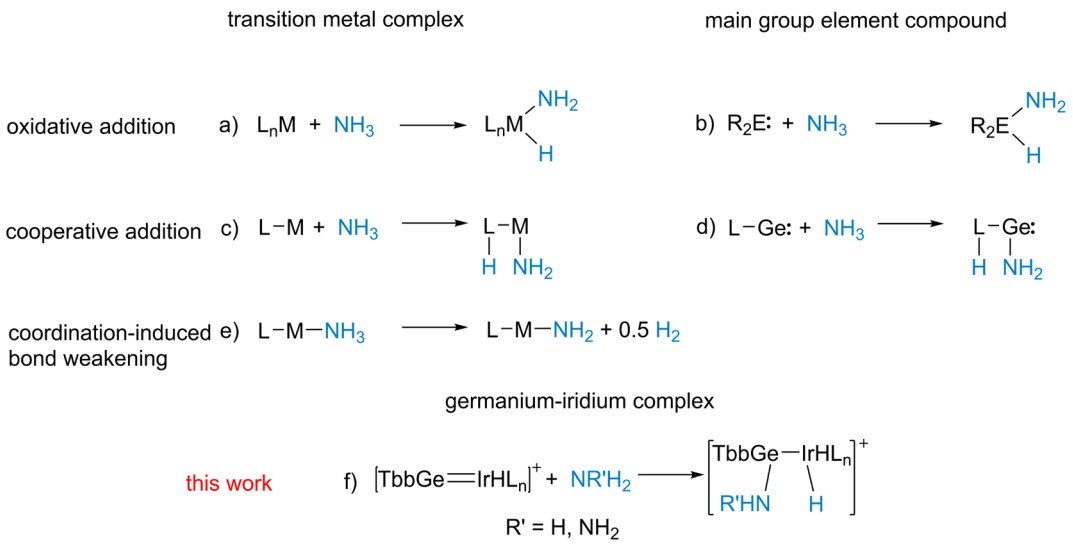

Scheme 5 Reactions of ammonia with transition metal complexes and main group element compounds.

element ligand reacting as an electrophile (Schemes 3 and 5f).[88] Metal–Lewis acid cooperativity was established for Lewis acidic triply coordinate aluminium or boron ligands and the coordination compounds were shown to activate hydrogen, water and C–H bonds.[86,89–94]

Both cations [Ge–Ir] **3** and [Sn–Ir] **4** add water in reaction with two equivalents of adduct $BaCl_2 \cdot H_2O$ in *o*-DFB. The $BaCl_2$ adduct of water was used because the much higher molecular weight of the adduct allows a much more precise weighing (based on NMR spectroscopy, in the case of **3** with an excess of water the same selective product formation was found). The water molecule exhibits a comparable reactivity like NH_3 and N_2H_4. In the product complexes [Ge–OH] **9** and [Sn–OH] **10** a hydroxide unit is bound at the Group 14 element and the proton is coordinated at the iridium atom. The molecular structure of the water addition at the germanium cation **9** is shown in Fig. 6 (structure of **10** see ESI†). The Ge–O distance found in complex **9** can be compared with a variety of organogermanium hydroxide structures.[95–98] The found hydroxide coordination compounds are rare examples for Group 14 element hydroxides of coordination number three.[97] Tetracoordinate low valent germanium and tin hydroxides, however, are well known in the literature.[99–103] Products **9** and **10** exhibit in the ^{1}H NMR spectrum a characteristic OH resonance (**9**: 5.29 ppm, d, $^4J_{PH} = 3.8$ Hz; **10**: 4.11 ppm, br. s). The signal in the ^{119}Sn NMR spectrum was observed at 648 ppm, lying in the range of the calculated isotropic shift of 778 ppm (see ESI† for details). Water addition at transition metal complexes was studied intensively and in the case of cooperative transition metal/Lewis base bond activation, the hydroxide forms a bond with the transition metal.[82,104–106] Figueroa *et al.* have presented an example for cooperative platinum/borane water activation. As found in the products **9** and **10**, in this platinum/borane example, the hydroxide forms a bond to the electrophilic ligand.[92]

Products of HCl addition **11a** and **12a** show in both cases protonation of the iridium atom and chloride addition to the Group 14 element (Scheme 3). The homologous bromide complex (**12b**) was synthesized by protonation of tetrylene coordination compound **2** with $[H(OEt_2)_2][BAr^F{}_4]$. The molecular structure of the cation of bromide **12b** is shown in the ESI.†

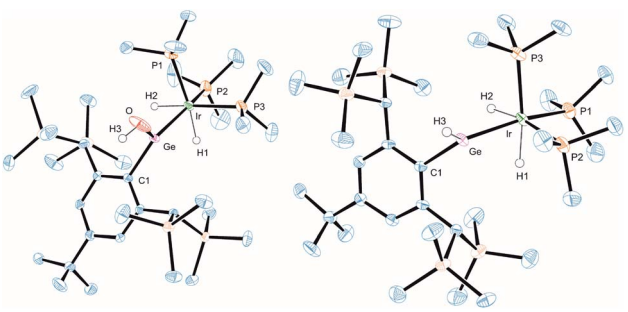

Fig. 6 ORTEP of the molecular structures of **9** and **13**. Ellipsoids set at 50% probability. Hydrogen atoms except OH, GeH, and Ir–H are omitted for clarity. For selected interatomic distances and angles see Table 2.

In the ^{1}H NMR spectrum for the IrH_2 moiety, a signal at low frequencies was observed (Table 1) and in the case of the tin product a signal in the ^{119}Sn NMR was found at 772 ppm (Table 1).

Cations [Ge–Ir] **3** and [Sn–Ir] **4** were also reacted with hydrogen at ambient temperatures and diverging reactivity with this unpolar substrate was found. The [Ge–Ir] **3** cation splits the hydrogen molecule to add a hydride at the germanium atom and a proton to the $[IrH(PMe_3)_3]$ moiety (Scheme 3, **13**). This type of cooperative transition metal/Lewis acid hydrogen activation was found only for transition metal–borane complexes so far.[92,107–110] In the tin case, we found a stepwise reaction: first addition of H_2 at iridium was observed (Scheme 3, **14**), which can be compared with hydrogenation of a rhodium–tin triple bond in the stannylidyne complex $[(Me_3P)_2(Ph_3P)Rh{\equiv}SnAr^*]$ [see Scheme 1 reaction (6)] adding one equivalent of hydrogen at rhodium to give $[(Me_3P)_2(Ph_3P)RhH_2{-}SnAr^*]$.[30] The iridium trihydride fragment $[Ir(H)_3(PMe_3)_3]$ of **14** (see Scheme 3 for depiction of **14**) shows high symmetry in solution even at −30 °C (because of the low solubility of **14**, NMR experiments below −30 °C were not possible): only one signal in the ^{1}H NMR spectrum for the IrH_3 unit at −7.94 ppm with tin satellites ($^1J_{Sn-H} = 265$ Hz) and one signal in the ^{31}P NMR spectrum (Table 1) were observed. The signal in the ^{119}Sn NMR spectrum was found at 1592 ppm. We interpret these spectroscopic findings, which can be compared with the hydride bridged Rh-complex $[Ar^*Sn(\mu\text{-}H_2)Rh(PPh_3)_2]$ [^{1}H: −4.13 ppm (J_{Sn-H} 220 Hz), ^{119}Sn 1728 ppm],[30] as an indicator for a triply hydride-bridged structure of **14** $[TbbSn(\mu\text{-}H_3)Ir(PMe_3)_3]^+$. This type of $[M(\mu\text{-}H_3)Ir(PEt_3)_3]^+$ structural motif is already known for a rhodium fragment [M = (dppe)Rh].[111] Remarkably, after one week, cation **14** undergoes a slow hydrogen shift of one hydrogen atom from the bridging position [Sn(μ-H)Ir] to the tin substituent to give **15** (Scheme 3). Obviously, the hydridostannylene coordination at iridium (**15**) is energetically favoured over the hydrido-bridged structure (**14**).[112–114] Complexes **13** and **15** are examples for hydridotetrylene coordination featuring a characteristic signal in the ^{1}H NMR spectrum for the coordinated TbbE-H moiety at high frequencies (Table 1, **13**: GeH 13.98 ppm; **15**: SnH 18.59 ppm).[23,42,113–117] The molecular structure of Ge-hydride **13** is shown in Fig. 6.

Finally, we also studied the addition of hydride (delivered by $K[HBEt_3]$) to the iridium–tetrylidinium cations **3** [Ge–Ir] and **4** [Sn–Ir] (Scheme 6). In the germanium case a mixture of two products was isolated: the hydridogermylene complex (**16**, 50%) and the hydridoirido-germylene (**17**, 50%). Both products can be reversibly converted *via* an 1,2-H shift into each other (Scheme 6, see ESI† for NMR spectra of the transfer). Hydridogermylene **16**, which is the more stable isomer, was converted under the influence of light (460 nm) into the irido-germylene **17** almost quantitatively. After 5 days gently heating at 40 °C the hydrogen atom is transferred back to the germanium to give **16** (at rt a 1 : 1 mixture with **17** was isolated). This type of reversible 1,2-H shift was also observed in the case of a tungsten–germylene complex.[118] Chemistry of hydrido(hydridotetrylene)coordination compounds was intensively studied by

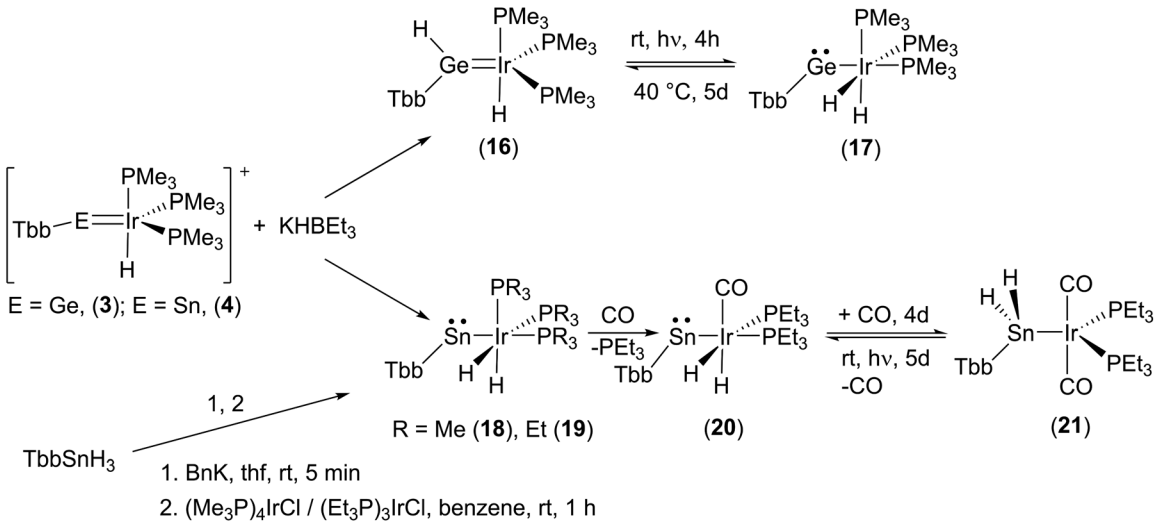

Scheme 6 Hydride addition at cations **3** and **4**. Reversible 1,2-H-shift reactions **16**–**17**, $h\nu = 460$ nm. Ligand induced hydrogen transfer **20**–**21**, $h\nu$ = UV-lamp.

Tobita and Tilley *et al.* for a variety of systems MH-EH (Mo–Ge,[25] W–Si,[116] W–Ge,[27,119] Ru–Si,[120] Os–Sn,[114] Ir–Si[42]).

To our surprise, the homologous tin cation **4** [Sn–Ir] adds the hydride almost exclusively at the iridium atom and only a slight amount of addition at the tin atom was observed by NMR spectroscopy in the course of the low temperature synthesis. An irido-stannylene (**18**) is formed, which was also synthesized with varying phosphines (**18**-PMe_3, **19**-PEt_3) by an alternative approach starting from the trihydride $TbbSnH_3$ (Scheme 6).[33] Deprotonation using benzyl-potassium yields [$TbbSnH_2K$] and is followed by reaction with the electrophile [$(R_3P)_nIrCl$] (R = Me $n = 4$, R = Et $n = 3$).[121,122] During this synthesis of complexes **18** and **19**, two hydrogen atoms show a 1,2-H shift from tin to iridium. Tilley *et al.* reported a stepwise 1,2-H shift of two hydrogen atoms from tin to iron, ruthenium, and osmium, respectively.[23,113,114]

The stability of hydridogermylene (**16**) and hydrido-metallostannylene (**18**) isomers goes along with findings from Tilley and co-workers.[112–114,123,124]

To investigate a possible transfer of the hydrogen atoms back to the tin, we started to exchange the phosphine ligands against carbonyl ligands. The aim was to destabilize the oxidation state three of iridium in complex **19** with the coordination of strong π-accepting ligands. Substitution by a second carbonyl ligand finally resulted in transfer of the hydrogen atoms back to the tin atom to yield a stannyl complex **21**. Remarkably, this ligand induced hydrogen transfer is a reversible reaction. Under the influence of light (UV-lamp) for 5 days the carbonyl is released and both hydrogen atoms are transferred back to the iridium atom to give metallostannylene **20** in a mixture with **21** (80 : 20) (Scheme 6, see ESI†). To the best of our knowledge this is a rare case for such a reversible ligand-induced transfer. Examples for the ligand-induced reductive elimination reactions were reported in the literature for alkane elimination from Zr(IV) or Pd(II) complexes,[125–127] hydrogen from dinuclear platinum compounds,[128] and arene from a tungsten complex.[129,130] Complexes **18**–**21** were characterized by NMR spectroscopy

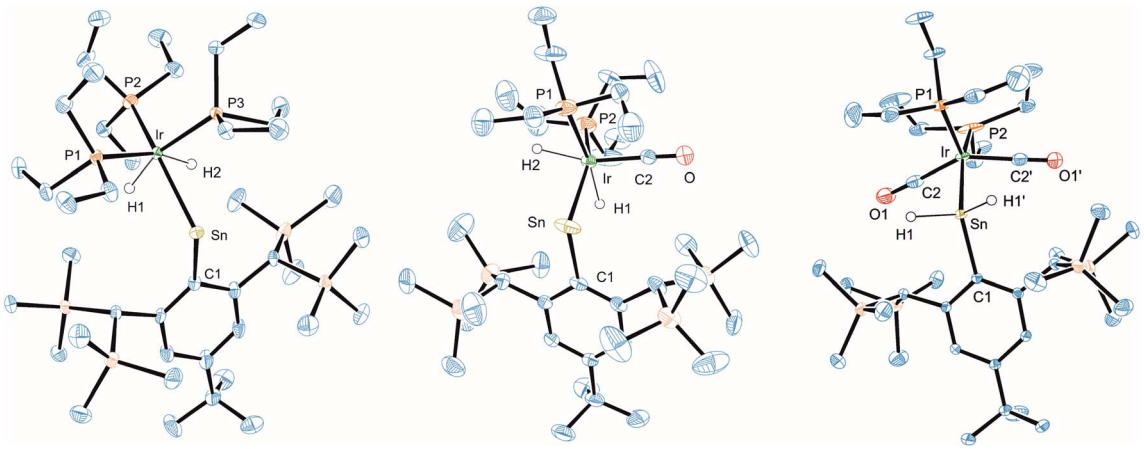

Fig. 7 ORTEP of the molecular structures of **19**, **20** and **21**. Ellipsoids set at 50% probability. Hydrogen atoms except SnH and Ir–H are omitted for clarity. For selected interatomic distances and angles see Table 2.

(Table 1) and molecular structures of **19–21** are shown in Fig. 7 (Table 2).

Conclusions

Tetrylidinium–iridium cations $[ArGe{=}IrHL_3]^+$ and $[ArSn{=}IrHL_3]^+$ show a vinyl-cation type bonding situation with a double bond between tetrylene and iridium atoms and an empty p-orbital at the Group 14 element. These tetrylidinium cations are highly reactive electrophiles acting as a cooperative metal–ligand Lewis acid. Selective addition of polar as well as nonpolar Z–H bonds ($Z = NH_2$, N_2H_3, OH, Cl, H) at the cationic moiety $[E = Ir]^+$ (E = Ge, Sn) was characterized.

The germylidinium cation adds hydride at the germanium atom and the product shows a reversible 1,2-H shift between the germanium [GeH–IrH] and iridium atom [Ge–IrH_2]. The tin cation adds a hydride exclusively at the iridium atom and the products of a reversible ligand induced transfer of two hydrogen atoms between tin [Sn–IrH_2] and iridium [SnH_2–Ir] were isolated after PEt_3/CO substitution reactions.

These findings stimulate for a more general study of cationic low valent main group element coordination at transition metals.

Data availability

Full experimental and computational details are provided as part of the ESI.†

Author contributions

Investigations, writing, original draft preparation, review M. A.; preparation of **1**, **5**, **9**, and **13** J. B.; special NMR experiments K. E.; discussion of X-ray measurements H. S.; DFT calculation, manuscript review C. P. S.; supervision, funding acquisition, DFT calculation, manuscript writing and review L. W.

Conflicts of interest

There are no conflicts to declare.

Acknowledgements

M. A. thanks the Fonds der Chemischen Industrie for a scholarship. We acknowledge support of the state of Baden-Württemberg through bwHPC and the German Research Foundation (DFG) through grant no INST 40/575-1 FUGG (Justus 2 Cluster).

Notes and references

1 H. Hashimoto and K. Nagata, *Chem. Lett.*, 2021, **50**, 778–787.
2 R. S. Simons and P. P. Power, *J. Am. Chem. Soc.*, 1996, **118**, 11966–11967.
3 L. Pu, B. Twamley, S. T. Haubrich, M. M. Olmstead, B. V. Mork, R. S. Simons and P. P. Power, *J. Am. Chem. Soc.*, 2000, **122**, 650–656.
4 P. Ghana, M. I. Arz, U. Chakraborty, G. Schnakenburg and A. C. Filippou, *J. Am. Chem. Soc.*, 2018, **140**, 7187–7198.
5 P. Ghana, M. I. Arz, G. Schnakenburg, M. Straßmann and A. C. Filippou, *Organometallics*, 2018, **37**, 772–780.
6 A. C. Filippou, D. Hoffmann and G. Schnakenburg, *Chem. Sci.*, 2017, **8**, 6290–6299.
7 A. C. Filippou, P. Ghana, U. Chakraborty and G. Schnakenburg, *J. Am. Chem. Soc.*, 2013, **135**, 11525–11528.
8 A. C. Filippou, U. Chakraborty and G. Schnakenburg, *Chem.–Eur. J.*, 2013, **19**, 5676–5686.
9 A. C. Filippou, A. Barandov, G. Schnakenburg, B. Lewall, M. van Gastel and A. Marchanka, *Angew. Chem., Int. Ed.*, 2012, **51**, 789–793.
10 A. C. Filippou, O. Chernov and G. Schnakenburg, *Chem.–Eur. J.*, 2011, **17**, 13574–13583.
11 A. C. Filippou, O. Chernov, K. W. Stumpf and G. Schnakenburg, *Angew. Chem., Int. Ed.*, 2010, **49**, 3296–3300.
12 A. C. Filippou, N. Weidemann and G. Schnakenburg, *Angew. Chem., Int. Ed.*, 2008, **47**, 5799–5802.
13 A. C. Filippou, N. Weidemann, A. I. Philippopoulos and G. Schnakenburg, *Angew. Chem.*, 2006, **118**, 6133–6137.
14 A. C. Filippou, N. Weidemann, G. Schnakenburg, H. Rohde and A. I. Philippopoulos, *Angew. Chem., Int. Ed.*, 2004, **43**, 6512–6516.
15 A. C. Filippou, H. Rohde and G. Schnakenburg, *Angew. Chem.*, 2004, **116**, 2293–2297.
16 A. C. Filippou, P. Portius, A. I. Philippopoulos and H. Rohde, *Angew. Chem., Int. Ed.*, 2003, **42**, 445–447.
17 A. C. Filippou, A. I. Philippopoulos and G. Schnakenburg, *Organometallics*, 2003, **22**, 3339–3341.
18 A. C. Filippou, P. Portius and A. I. Philippopoulos, *Organometallics*, 2002, **21**, 653–661.
19 A. C. Filippou, A. I. Philippopoulos, P. Portius and D. U. Neumann, *Angew. Chem., Int. Ed.*, 2000, **39**, 2778–2781.
20 J. Hicks, T. J. Hadlington, C. Schenk, J. Li and C. Jones, *Organometallics*, 2013, **32**, 323–329.
21 B. V. Mork and T. D. Tilley, *Angew. Chem., Int. Ed.*, 2003, **42**, 357–360.
22 P. G. Hayes, Z. Xu, C. Beddie, J. M. Keith, M. B. Hall and T. D. Tilley, *J. Am. Chem. Soc.*, 2013, **135**, 11780–11783.
23 R. C. Handford, M. A. Nesbit, P. W. Smith, R. D. Britt and T. D. Tilley, *J. Am. Chem. Soc.*, 2022, **144**, 358–367.
24 P. M. Keil and T. J. Hadlington, *Chem. Commun.*, 2022, **58**, 3011–3014.
25 T. P. Dhungana, H. Hashimoto, M. Ray and H. Tobita, *Organometallics*, 2020, **39**, 4350–4361.
26 T. Fukuda, T. Yoshimoto, H. Hashimoto and H. Tobita, *Organometallics*, 2016, **35**, 921–924.
27 H. Hashimoto, T. Fukuda, H. Tobita, M. Ray and S. Sakaki, *Angew. Chem., Int. Ed.*, 2012, **51**, 2930–2933.
28 T. Fukuda, H. Hashimoto and H. Tobita, *J. Organomet. Chem.*, 2017, **848**, 89–94.
29 J. D. Queen, A. C. Phung, C. A. Caputo, J. C. Fettinger and P. P. Power, *J. Am. Chem. Soc.*, 2020, **142**, 2233–2237.

30 M. Widemann, K. Eichele, H. Schubert, C. P. Sindlinger, S. Klenner, R. Pöttgen and L. Wesemann, *Angew. Chem., Int. Ed.*, 2021, **60**, 5882–5889.
31 D. L. Thorn and T. H. Tulip, *Organometallics*, 1982, **1**, 1580–1586.
32 T. Sasamori, T. Sugahara, T. Agou, J.-D. Guo, S. Nagase, R. Streubel and N. Tokitoh, *Organometallics*, 2015, **34**, 2106–2109.
33 M. Auer, F. Diab, K. Eichele, H. Schubert and L. Wesemann, *Dalton Trans.*, 2022, **51**, 5950–5961.
34 J. D. Feldman, J. C. Peters and T. D. Tilley, *Organometallics*, 2002, **21**, 4065–4075.
35 N. A. Bell, F. Glockling, M. L. Schneider, H. M. M. Shearer and M. D. Wilbey, *Acta Crystallogr., Sect. C: Struct. Chem.*, 1984, **40**, 625–628.
36 S. M. Hawkins, P. B. Hitchcock, M. F. Lappert and A. K. Rai, *Chem. Commun.*, 1986, 1689–1690.
37 E. D. Glendening, J. K. Badenhoop, A. E. Reed, J. E. Carpenter, J. A. Bohmann, C. M. Morales, P. Karafiloglou, C. R. Landis and F. Weinhold, *NBO 7.0*, 2018.
38 F. Neese, F. Wennmohs, U. Becker and C. Riplinger, *J. Chem. Phys.*, 2020, **152**, 224108.
39 F. Neese, *Wiley Interdiscip. Rev.: Comput. Mol. Sci.*, 2012, **2**, 73–78.
40 J. Henoch, A. Auch, F. Diab, K. Eichele, H. Schubert, P. Sirsch, T. Block, R. Pöttgen and L. Wesemann, *Inorg. Chem.*, 2018, **57**, 4135–4145.
41 K. M. Krebs, S. Freitag, H. Schubert, B. Gerke, R. Pöttgen and L. Wesemann, *Chem.–Eur. J.*, 2015, **21**, 4628–4638.
42 R. S. Simons, J. C. Gallucci, C. A. Tessier and W. J. Youngs, *J. Organomet. Chem.*, 2002, **654**, 224–228.
43 E. Calimano and T. D. Tilley, *J. Am. Chem. Soc.*, 2008, **130**, 9226–9227.
44 J. A. Cabeza, J. M. Fernández-Colinas, P. García-Álvarez, L. González-Álvarez and E. Pérez-Carreño, *Dalton Trans.*, 2019, **48**, 10996–11003.
45 T. J. Malosh, J. R. Shapley, R. J. Lawson, D. N. T. Hay and T. N. Rohrabaugh, *J. Organomet. Chem.*, 2013, **745–746**, 98–105.
46 R. D. Adams, Y. Kan and Q. Zhang, *Organometallics*, 2011, **30**, 328–333.
47 R. D. Adams, M. Chen, E. Trufan and Q. Zhang, *Organometallics*, 2011, **30**, 661–664.
48 T. W. Dingle and K. R. Dixon, *Inorg. Chem.*, 1974, **13**, 846–851.
49 P. Diehl and J. A. Pople, *Mol. Phys.*, 1960, **3**, 557–561.
50 R. J. Abraham, E. O. Bishop and R. E. Richards, *Mol. Phys.*, 1960, **3**, 485–494.
51 K. Bakthavachalam, S. Dutta, C. Arivazhagan, B. Raghavendra, A. Haridas, S. S. Sen, D. Koley and S. Ghosh, *Dalton Trans.*, 2018, **47**, 15835–15844.
52 A. Jana, H. W. Roesky, C. Schulzke, P. P. Samuel and A. Döring, *Inorg. Chem.*, 2010, **49**, 5554–5559.
53 Z. D. Brown, J.-D. Guo, S. Nagase and P. P. Power, *Organometallics*, 2012, **31**, 3768–3772.
54 A. Hinz, *Chem.–Eur. J.*, 2019, **25**, 7843–7846.
55 A. Jana, I. Objartel, H. W. Roesky and D. Stalke, *Inorg. Chem.*, 2009, **48**, 798–800.
56 M. Usher, A. V. Protchenko, A. Rit, J. Campos, E. L. Kolychev, R. Tirfoin and S. Aldridge, *Chem.–Eur. J.*, 2016, **22**, 11685–11698.
57 Y. Peng, J.-D. Guo, B. D. Ellis, Z. Zhu, J. C. Fettinger, S. Nagase and P. P. Power, *J. Am. Chem. Soc.*, 2009, **131**, 16272–16282.
58 A. Jana, S. S. Sen, H. W. Roesky, C. Schulzke, S. Dutta and S. K. Pati, *Angew. Chem., Int. Ed.*, 2009, **48**, 4246–4248.
59 L. Nurdin, Y. Yang, P. G. N. Neate, W. E. Piers, L. Maron, M. L. Neidig, J.-B. Lin and B. S. Gelfand, *Chem. Sci.*, 2021, **12**, 2231–2241.
60 M. J. Bezdek, S. Guo and P. J. Chirik, *Science*, 2016, **354**, 730–733.
61 G. W. Margulieux, M. J. Bezdek, Z. R. Turner and P. J. Chirik, *J. Am. Chem. Soc.*, 2017, **139**, 6110–6113.
62 J. I. van der Vlugt, *Chem. Soc. Rev.*, 2010, **39**, 2302–2322.
63 M. G. Scheibel, J. Abbenseth, M. Kinauer, F. W. Heinemann, C. Würtele, B. de Bruin and S. Schneider, *Inorg. Chem.*, 2015, **54**, 9290–9302.
64 G. P. Connor, D. Delony, J. E. Weber, B. Q. Mercado, J. B. Curley, S. Schneider, J. M. Mayer and P. L. Holland, *Chem. Sci.*, 2022, **13**, 4010–4018.
65 A. L. Casalnuovo, J. C. Calabrese and D. Milstein, *Inorg. Chem.*, 1987, **26**, 971–973.
66 J. Zhao, A. S. Goldman and J. F. Hartwig, *Science*, 2005, **307**, 1080–1082.
67 E. Morgan, D. F. MacLean, R. McDonald and L. Turculet, *J. Am. Chem. Soc.*, 2009, **131**, 14234–14236.
68 C. M. Fafard, D. Adhikari, B. M. Foxman, D. J. Mindiola and O. V. Ozerov, *J. Am. Chem. Soc.*, 2007, **129**, 10318–10319.
69 M. P. Betoré, M. A. Casado, P. García-Orduña, F. J. Lahoz, V. Polo and L. A. Oro, *Organometallics*, 2016, **35**, 720–731.
70 G. D. Frey, V. Lavallo, B. Donnadieu, W. W. Schoeller and G. Bertrand, *Science*, 2007, **316**, 439–441.
71 Y. Peng, B. D. Ellis, X. Wang and P. P. Power, *J. Am. Chem. Soc.*, 2008, **130**, 12268–12269.
72 P. A. Chase and D. W. Stephan, *Angew. Chem., Int. Ed.*, 2008, **47**, 7433–7437.
73 Z. Zhu, X. Wang, Y. Peng, H. Lei, J. C. Fettinger, E. Rivard and P. P. Power, *Angew. Chem., Int. Ed.*, 2009, **48**, 2031–2034.
74 A. Jana, C. Schulzke and H. W. Roesky, *J. Am. Chem. Soc.*, 2009, **131**, 4600–4601.
75 A. Meltzer, S. Inoue, C. Präsang and M. Driess, *J. Am. Chem. Soc.*, 2010, **132**, 3038–3046.
76 S. M. McCarthy, Y.-C. Lin, D. Devarajan, J. W. Chang, H. P. Yennawar, R. M. Rioux, D. H. Ess and A. T. Radosevich, *J. Am. Chem. Soc.*, 2014, **136**, 4640–4650.
77 J. Cui, Y. Li, R. Ganguly, A. Inthirarajah, H. Hirao and R. Kinjo, *J. Am. Chem. Soc.*, 2014, **136**, 16764–16767.
78 T. P. Robinson, D. M. De Rosa, S. Aldridge and J. M. Goicoechea, *Angew. Chem., Int. Ed.*, 2015, **54**, 13758–13763.
79 A. V. Protchenko, J. I. Bates, L. M. A. Saleh, M. P. Blake, A. D. Schwarz, E. L. Kolychev, A. L. Thompson, C. Jones,

P. Mountford and S. Aldridge, *J. Am. Chem. Soc.*, 2016, **138**, 4555–4564.
80 D. C. H. Do, A. V. Protchenko, M. Á. Fuentes, J. Hicks, P. Vasko and S. Aldridge, *Chem. Commun.*, 2020, **56**, 4684–4687.
81 E. Khaskin, M. A. Iron, L. J. W. Shimon, J. Zhang and D. Milstein, *J. Am. Chem. Soc.*, 2010, **132**, 8542–8543.
82 D. V. Gutsulyak, W. E. Piers, J. Borau-Garcia and M. Parvez, *J. Am. Chem. Soc.*, 2013, **135**, 11776–11779.
83 Y.-H. Chang, Y. Nakajima, H. Tanaka, K. Yoshizawa and F. Ozawa, *J. Am. Chem. Soc.*, 2013, **135**, 11791–11794.
84 R. M. Brown, J. Borau Garcia, J. Valjus, C. J. Roberts, H. M. Tuononen, M. Parvez and R. Roesler, *Angew. Chem., Int. Ed.*, 2015, **54**, 6274–6277.
85 C. Gunanathan and D. Milstein, *Acc. Chem. Res.*, 2011, **44**, 588–602.
86 M. R. Elsby and R. T. Baker, *Chem. Soc. Rev.*, 2020, **49**, 8933–8987.
87 O. Chernov, Dissertation, Rheinische Friedrich-Wilhelms-University of Bonn, 2012.
88 R. J. Somerville and J. Campos, *Eur. J. Inorg. Chem.*, 2021, **2021**, 3488–3498.
89 G. Bouhadir and D. Bourissou, *Chem. Soc. Rev.*, 2016, **45**, 1065–1079.
90 A. Maity and T. S. Teets, *Chem. Rev.*, 2016, **116**, 8873–8911.
91 N. Gorgas, A. J. P. White and M. R. Crimmin, *J. Am. Chem. Soc.*, 2022, **144**, 8770–8777.
92 B. R. Barnett, C. E. Moore, A. L. Rheingold and J. S. Figueroa, *J. Am. Chem. Soc.*, 2014, **136**, 10262–10265.
93 D. You and F. P. Gabbaï, *J. Am. Chem. Soc.*, 2017, **139**, 6843–6846.
94 L. Escomel, I. Del Rosal, L. Maron, E. Jeanneau, L. Veyre, C. Thieuleux and C. Camp, *J. Am. Chem. Soc.*, 2021, **143**, 4844–4856.
95 L. Pu, N. J. Hardman and P. P. Power, *Organometallics*, 2001, **20**, 5105–5109.
96 L.-C. Pop, N. Kurokawa, H. Ebata, K. Tomizawa, T. Tajima, M. Ikeda, M. Yoshioka, M. Biesemans, R. Willem, M. Minoura and M. Saito, *Can. J. Chem.*, 2014, **92**, 542–548.
97 W.-P. Leung, K.-W. Kan, Y.-C. Chan and T. C. W. Mak, *Inorg. Chem.*, 2013, **52**, 4571–4577.
98 A. C. Filippou, K. W. Stumpf, O. Chernov and G. Schnakenburg, *Organometallics*, 2012, **31**, 748–755.
99 P. Nie, Y. Li, Q. Yu, B. Li, H. Zhu and T.-B. Wen, *Eur. J. Inorg. Chem.*, 2017, **2017**, 3892–3899.
100 C. Bibal, S. Mazières, H. Gornitzka and C. Couret, *Organometallics*, 2002, **21**, 2940–2943.
101 R. Jambor, B. Kašná, S. G. Koller, C. Strohmann, M. Schürmann and K. Jurkschat, *Eur. J. Inorg. Chem.*, 2010, **2010**, 902–908.
102 L. W. Pineda, V. Jancik, J. F. Colunga-Valladares, H. W. Roesky, A. Hofmeister and J. Magull, *Organometallics*, 2006, **25**, 2381–2383.
103 A. Jana, S. P. Sarish, H. W. Roesky, C. Schulzke and P. P. Samuel, *Chem. Commun.*, 2010, **46**, 707–709.
104 D. Morales-Morales, D. W. Lee, Z. Wang and C. M. Jensen, *Organometallics*, 2001, **20**, 1144–1147.
105 P. Kläring, S. Pahl, T. Braun and A. Penner, *Dalton Trans.*, 2011, **40**, 6785–6791.
106 O. V. Ozerov, *Chem. Soc. Rev.*, 2009, **38**, 83–88.
107 N. Tsoureas, Y.-Y. Kuo, M. F. Haddow and G. R. Owen, *Chem. Commun.*, 2011, **47**, 484–486.
108 W. H. Harman and J. C. Peters, *J. Am. Chem. Soc.*, 2012, **134**, 5080–5082.
109 H. Fong, M.-E. Moret, Y. Lee and J. C. Peters, *Organometallics*, 2013, **32**, 3053–3062.
110 B. E. Cowie and D. J. H. Emslie, *Chem.–Eur. J.*, 2014, **20**, 16899–16912.
111 A. Albinati, A. Musco, R. Naegeli and L. M. Venanzi, *Angew. Chem., Int. Ed.*, 1981, **20**, 958–959.
112 P. W. Smith, R. C. Handford and T. D. Tilley, *Organometallics*, 2019, **38**, 4060–4065.
113 H.-J. Liu, J. Guihaumé, T. Davin, C. Raynaud, O. Eisenstein and T. D. Tilley, *J. Am. Chem. Soc.*, 2014, **136**, 13991–13994.
114 P. G. Hayes, C. W. Gribble, R. Waterman and T. D. Tilley, *J. Am. Chem. Soc.*, 2009, **131**, 4606–4607.
115 M. E. Fasulo and T. D. Tilley, *Chem. Commun.*, 2012, **48**, 7690–7692.
116 T. Watanabe, H. Hashimoto and H. Tobita, *Angew. Chem., Int. Ed.*, 2004, **43**, 218–221.
117 Q. Zhu, J. C. Fettinger and P. P. Power, *Dalton Trans.*, 2021, **50**, 12555–12562.
118 M. Widemann, S. Jeggle, M. Auer, K. Eichele, H. Schubert, C. P. Sindlinger and L. Wesemann, *Chem. Sci.*, 2022, **13**, 3999–4009.
119 H. Hashimoto, T. Tsubota, T. Fukuda and H. Tobita, *Chem. Lett.*, 2009, **38**, 1196–1197.
120 M. Ochiai, H. Hashimoto and H. Tobita, *Angew. Chem., Int. Ed.*, 2007, **46**, 8192–8194.
121 R. S. Simons, J. C. Gallucci, C. A. Tessier and W. J. Youngs, *J. Organomet. Chem.*, 2002, **654**(1), 224–228.
122 T. Herskovitz, C. Kampe, H. D. Kaesz and W. M. Seidel, *Inorg. Synth.*, 1982, 99–103.
123 H.-J. Liu, C. Landis, C. Raynaud, O. Eisenstein and T. D. Tilley, *J. Am. Chem. Soc.*, 2015, **137**, 9186–9194.
124 P. G. Hayes, R. Waterman, P. B. Glaser and T. D. Tilley, *Organometallics*, 2009, **28**, 5082–5089.
125 K. I. Gell and J. Schwartz, *J. Am. Chem. Soc.*, 1981, **103**, 2687–2695.
126 M. Tanabe, N. Ishikawa and K. Osakada, *Organometallics*, 2006, **25**, 796–798.
127 S. Otsuka, T. Yoshida, M. Matsumoto and K. Nakatsu, *J. Am. Chem. Soc.*, 1976, **98**, 5850–5858.
128 R. H. Hill and R. J. Puddephatt, *J. Am. Chem. Soc.*, 1983, **105**, 5797–5804.
129 D. J. Burkey, J. D. Debad and P. Legzdins, *J. Am. Chem. Soc.*, 1997, **119**, 1139–1140.
130 D. M. Crumpton-Bregel and K. I. Goldberg, *J. Am. Chem. Soc.*, 2003, **125**, 9442–9456.